Talanta Open 7 (2023) 100202

Contents lists available at ScienceDirect

Talanta Open

journal homepage: www.sciencedirect.com/journal/talanta-open

Highly selective and sensitive fluorescent determination of Fe^{3+} within alcoholic beverages with 1,5-diphenylcarbazone-functionalized graphene quantum dots

Mauricio Llaver [a,*], Santiago D. Barrionuevo [b], Horacio Troiani [c], Rodolfo G. Wuilloud [a], Francisco J. Ibañez [b,*]

[a] Laboratorio de Química Analítica para Investigación y Desarrollo (QUIANID), Facultad de Ciencias Exactas y Naturales, Universidad Nacional de Cuyo / Instituto Interdisciplinario de Ciencias Básicas (ICB), CONICET UNCUYO, Padre J. Contreras 300, (5500), Mendoza, Argentina
[b] Instituto de Investigaciones Fisicoquímicas, Teóricas y Aplicadas (INIFTA), Universidad Nacional de La Plata - CONICET. Sucursal 4 Casilla de Correo 16, (1900), La Plata, Argentina
[c] Centro Atómico Bariloche, Consejo Nacional de Investigaciones Científicas y Técnicas (CONICET), Av. Bustillo 9500, S.C. de Bariloche, Rio Negro CP 8400, Argentina

ARTICLE INFO

Keywords:
Fluorescence probe
Environmental samples
Wine analysis
Analytical method
Water analysis
Nanomaterial

ABSTRACT

Herein, we report the synthesis of graphene quantum dots (GQDs) functionalized with 1,5-diphenylcarbazone for the selective quantification of Fe in wine, via front-face fluorescence. Crystalline GQDs are obtained via a clean and relatively size-controlled synthesis based on the electrochemical exfoliation from a graphene foam. The product of the synthesis was later functionalized to solely detect Fe^{3+} amongst various other ions present within the sample. The detection is based on quenching the fluorescence emission from the functionalized nanomaterial in the presence of the analyte, which follows a linear relationship with the concentration of the analyte, consistent with the Stern-Volmer model. Diverse parameters involved in the measurements, including the pH and excitation wavelength, were optimized, giving place to limits of detection (LOD) of 0.014 mg L^{-1} and 0.11 mg L^{-1} in waters and white wines, respectively. A soft UV-based digestion and a profound analysis of interferences were key factors to achieve such LODs. Furthermore, front-face fluorescence measurements improved the applicability of the method by avoiding the commonly occurring matrix shielding effects. We believe that the sensitive, selective, and fast detection of Fe^{3+} within real (i.e.; wine) samples represents a major step forward in the field.

Introduction

The outstanding optical, electrical, and overall chemical properties of graphene quantum dots (GQDs) are special attributes due to quantum confinement and functional groups at the border [1]. As a consequence, these carbon nanostructures have been employed in a wide array of fields, ranging from cancer diagnostics to energy storage [2–4]. Among these, optical sensing applications involving detection by direct fluorescence quenching [5], Förster resonance energy transfer (FRET) [6] and fluorescence enhancement [7] have become valuable analytical tools in recent years. The synthesis of GQDs can proceed via two general approaches: bottom-up, which is based on building up molecule by molecule [8], and top-down methods, generally involving the breakdown (into small pieces) of bulk precursors. The latter comprise solvo- or hydrothermal cutting, ultrasonic exfoliation, acidic or plasma oxidation, or nanolithography, among others, to achieve the breakdown of the starting material [9]. Top-down methods performed from nanomaterials are specially interesting since they can give place to highly crystalline GQDs with relatively high control over the size of the product (i.e.; number of layers) [10,11], while avoiding the use of strong and hazardous chemical conditions [12].

GQDs are actually one step forward with respect to graphene because they exhibit a HOMO-LUMO bandgap that results in extraordinary optical properties [13]. Consequently, applications of GQDs for fluorescence sensing have grown notably in the last years, stimulated by the fact that they represent an attractive and more sustainable alternative to organic fluorophores, fluorescent metallic nanoclusters, and semiconducting quantum dots, given their superior photostability and

* Corresponding authors.
E-mail addresses: mllaver@mendoza-conicet.gob.ar (M. Llaver), fjiban@inifta.unlp.edu.ar (F.J. Ibañez).

https://doi.org/10.1016/j.talo.2023.100202
Received 24 January 2023; Received in revised form 3 March 2023; Accepted 5 March 2023
Available online 7 March 2023

biocompatibility [4]. In this context, metal ions are widely explored analytes because of their ability to quench the emission of GQDs via electron transfer mechanisms [14]. With the aim of improving the sensitivity, great progress has been achieved mainly associated with enhancements in the quantum yield of the probes [15]. For example, analytes including iodide [16], cyanide [17], melamine [18], and nitrite [19] within foods and beverage samples have been detected with similar fluorescence-based probes. Nevertheless, while sensitivity has been improved in aqueous samples [5], selectivity still presents major challenges, thus remaining one of the main factor hindering the direct application of GQD-based fluorescence sensors in complex matrices.

In this context, researchers are searching for more sensitive and selective carbon-based probes for the determination of Fe within wine samples. This is motivated by the fact that the quality and safety of oenological products -especially wine-, depends strongly on the concentration of inorganic ions in its composition. These may come from various sources, including raw materials and processing practices such as adding new ingredients for improving organoleptic properties [20]. Hence, the determination of these species in wine is of significant importance, since they can reveal information concerning their origin, conditions of cultivation and manufacture, as well as potential contaminations or added ingredients [21]. Furthermore, mineral content frequently causes precipitation and a subsequent loss of organoleptic properties [22]. It is clear then, that the determination of some critical metallic species, such as those of Fe, becomes paramount.

Although there are some reports that describe the use of GQDs for the detection of Fe^{3+}, many of them either present the analytical application as a secondary proof-of-concept application [23–25], or just deal with simple matrices in which organic and/or biological interferences do not have to be considered [26–30]. This work seeks for efficient alternatives to apply GQDs-based sensors beyond water analysis, where applications are scarce due to their inherently low selectivity. We hereby present the synthesis of 1,5-diphenylcarbazone-functionalized GQDs (DPC-GQDs), and their application as a fluorescence probe for the selective and sensitive determination of Fe^{3+} in environmental waters and of total Fe in white wine samples. The GQDs were initially obtained by an electrochemical exfoliation approach from graphene, characterized by high-resolution transmission electron microscopy (HR-TEM), and further functionalized with 1,5-diphenylcarbazone (1,5-DPC) via a wet chemistry method. The resulting nanomaterial was characterized by different techniques and successfully applied for the fast quantification of Fe^{3+} using a front-face fluorescence approach. Fe species within samples taken from river, dam, tap waters, and white wines were detected and carefully analyzed. To achieve high sensitivity and selectivity, several parameters such as pH, heating, UV exposure, and concentration of the probe were evaluated to optimize the fluorescence measurements and the digestion of wine samples. To the best of our knowledge, this represents the first application of GQDs for the fluorescent detection of elemental analytes in wine samples.

Materials and methods

Materials and reagents

Nickel foam with thickness = 1.6 mm and porosity = 87% was purchased from MTI Corp (Richmond, CA, USA). H_2 (99.999%) and CH_4 (99.999%) were purchased locally from Linde, Argentina. 1,5-diphenylcarbazide (1,5-DPCZ, > 98%) was from Riedel-de Haën, acetone (99.8%) and tris(hydroxymethyl)aminomethane (TRIS, > 98%) were from J.T. Baker, while sodium nitrate ($NaNO_3$, ≥ 99.0%) was from Sigma-Aldrich. Hydrogen peroxide (H_2O_2, 30% v/v) and nitric acid (HNO_3, 65% v/v) were from Merck. A 1000 mg L^{-1} Fe^{3+} standard solution from J.T. Baker was used for the preparation of working solutions. Standard solutions for interference assays were obtained from Merck and J.T. Baker. Ethyl acetate (99.8%) was from Sigma-Aldrich, and potassium thiocyanate (KSCN, 99%) was from Dalton (Mendoza, Argentina).

Instrumentation

Fluorescence measurements were carried out with a RF-6000 spectrofluorophotometer (Shimadzu, Kyoto, Japan). Front-face fluorescence spectra were collected using a quartz cuvette held by a solid sample holder including a light cutting filter for blocking scattered light. Spectra were smoothed using the Savitzky-Golay method with a 5-point window and a polynomial order of 2, using the OriginPro 2021 software (OriginLab Corporation). Excitation-emission matrices were obtained using the 3D built-in method included in the LabSolutions RF software (Shimadzu). Imaging of nanostructures and structural characterization was performed by HR-TEM, using a TECNAI F20 (FEI, Oregon, USA) microscope operating at 200 kV at room temperature. GQD dispersions used for this characterization were centrifuged at 10,000 rpm for 30 min, and the resulting clear supernatant was drop-casted onto the HR-TEM grids. No dialysis or chromatographic purification were performed on any of the samples. Attenuated Total Reflectance-Fourier Transform-Infrared (ATR-FT-IR) spectra were obtained using a Perkin Elmer (Beaconsfield, UK) Spectrum Two instrument with a Universal ATR module from the same company. UV–Vis spectroscopy measurements were carried out in a Shimadzu UV 1800 spectrophotometer using a standard quartz cuvette. A Horiba F-51 pH meter (Kyoto, Japan) was used for pH determinations. Ultrapure water (18 MΩ cm) was obtained from a Milli-Q water purification system (APEMA, Buenos Aires, Argentina).

Electrochemical exfoliation of graphene to obtain GQDs

GQDs were obtained following a relatively unexplored synthesis based on the electrochemical exfoliation of graphene grown on Ni foam by a well-known chemical vapor deposition method [31], as recently described [32]. Briefly, the electrochemical synthesis consisted on the application of a fixed voltage (30 V) to a graphene-covered Ni foam/Cu foil two-electrode system immersed in a NaOH ethanoic solution. The product of the synthesis was subjected to purification by three redissolution-centrifugation cycles, and finally stored as a powder at 4 °C.

Functionalization of GQDs with 1,5-DPC

The functionalization of GQDs with 1,5-diphenylcarbazone (1,5-DPC) was carried out using an aqueous solution of GQDs containing 120.0 mg of the material in 60 mL of ultrapure water. This solution was then mixed with 120.0 mg of 1,5-diphenylcarbazide (1,5-DPCZ) previously dissolved in 30 mL of acetone, and left to react during 24 h at room temperature under constant stirring. Throughout the reaction, the solution gradually turned purple, indicating the oxidation of 1,5-DPCZ into 1,5-DPC, as reported to occur in diverse reaction conditions [33, 34]. Afterwards, the mixture was left at 60 °C to evaporate the solvent, and the remaining solid was then washed 4 times with 10 mL of acetone, followed by centrifugation at 1080 xg during 15 min to remove all excess by-products. Finally, the purified solid was dried at room temperature and stored at 4 °C prior to its characterization and analytical application.

Collection of real samples and treatment

River and dam water samples were collected directly in clean HDPE bottles at 5 cm below the surface, whereas tap water was left to run for 20 min and sampled directly in a clean beaker. 500 mL of river waters from the Potrerillos dam (Mendoza, Argentina) and the La Carolina River (San Luis, Argentina) were collected, centrifuged to eliminate sand residues, and stored at −18 °C. Prior to their use, the aliquots from these samples were filtered through 0.45 μm pore size PTFE membrane filters.

In all cases, 50 μL of 2.0 mol L^{-1} TRIS buffer was added to the samples before the addition of the probe and fluorescence measurements. White wine samples, on the other hand, were purchased from markets of the City of Mendoza (Argentina) and were subjected to a soft digestion before the application of the fluorescent probe. A modified digestion protocol based on the one reported by dos Santos et al. [22] was followed, which consisted in the addition of 50 μL of 65% (v/v) HNO_3 and 50 μL of 30% (v/v) H_2O_2 to 5.00 mL of sample, followed by 2 h of irradiation with a low-power 15 W commercial lamp, with a maximum emission intensity at 253.7 nm, according to the manufacturer. The digested samples were then transferred to 10 mL volumetric flasks, and the pH was set to 9.0 using solid NaOH and 100 μL of a 2.0 mol L^{-1} TRIS

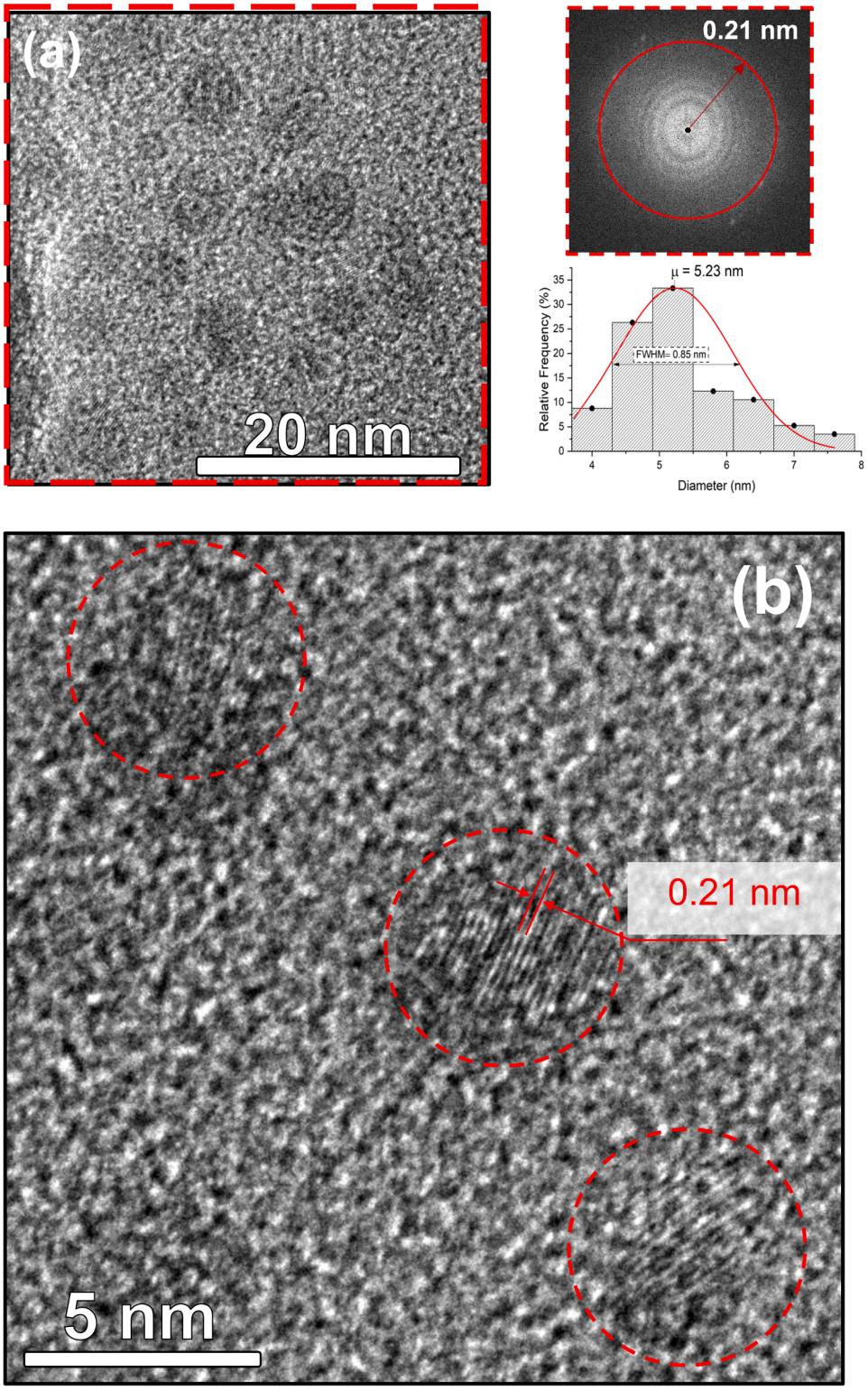

Fig. 1. (a) High-resolution transmission electron microscopy (HR-TEM) image of as-synthesized graphene quantum dots (GQDs), with its corresponding Fast Fourier Transform of a region of interest and their size distribution histogram. (b) Zoom-in HR-TEM image of as-synthesized GQDs.

buffer. For pH optimization studies, a phosphate buffer was used for adjusting the pH to 7.0 (final concentration = 0.02 mol L^{-1}), an acetic acid/acetate buffer for adjusting the pH to 4.0 (final concentration = 0.02 mol L^{-1}), while HCl was used for adjusting the pH to 1.0.

In all cases, fluorescence analyses were run on the samples after their pre-treatment, or on 5.00 mL aliquots of standard solutions prepared with 50 μL of 2.0 mol L^{-1} TRIS buffer in the case of optimization studies. 50 μL of 3.00 mg mL^{-1} aqueous GQD-DPCs were then added, and the mixtures were immediately measured by front-face fluorescence with the instrumental setup described in the *Instrumentation* section. Measurements were carried out in the emission range between 330 and 530 nm, with an excitation wavelength of 321 nm. The excitation and emission slits were fixed at 5.0 and 20 nm, respectively, to maximize the sensitivity, and the scan rate was 600 nm min^{-1} in all measurements, allowing for the measurement of full spectra in ca. 20 s.

Results and discussion

Characterization of GQDs and DPC-GQDs

Fig. 1(a) shows an HR-TEM image and the Fast Fourier Transform (FFT) taken from a group of as-synthesized GQDs. GQDs exhibit a highly crystalline structure with diameters ranging from 4.0 to 6.5 nm. Assessment on the crystallinity of the observed GQDs shows several spots in the diffraction pattern with a reciprocal vector of 4.76 nm^{-1}, commonly attributed to $01\bar{1}0$, $10\bar{1}0$, $1\bar{1}00$, $0\bar{1}10$, $\bar{1}010$, $\bar{1}100$ reflections for graphene-like nanostructures. Furthermore, the size distribution of the as-synthesized GQDs is shown as an inset, and it corresponds to a monomodal narrow gaussian distribution centered at 5.2 nm, with a 0.85 nm full-width half-maximum. Fig. 1(b) shows a 25 x 25 nm zoom-in HR-TEM image of the as-synthesized GQDs. Highly crystalline GQDs with diameters of ~ 5 nm are observed. Additionally, a lattice fringe of ~0.21 nm, assigned to the $10\bar{1}0$ reflection plane of graphene is measured and shown [35]. Further characterization of the electrochemically-obtained GQDs used as starting material, including Raman spectroscopy, atomic force microscopy (AFM) and X-ray photoelectron spectroscopy (XPS) can be found in a previously published work from our group [32].

Fig. 2 shows ATR-FT-IR spectra measured for GQDs before and after their functionalization, for the solid by-product obtained after drying the supernatant (assumed to be unreacted 1,5-DPC), and for the starting 1,5-DPCZ. The spectrum of the pristine GQDs shows typical signals at 1430 and 880 cm^{-1} (epoxide and ether groups) and at 1583 cm^{-1} (C = O stretching) [25,36]. There are some interesting aspects worth highlighting from the spectra corresponding to the functionalized probe. First, the appearance of several low-intensity signals in the region between 900 and 1200 cm^{-1}, along with a small shoulder at 1485 cm^{-1}, and the broadening of the band at 1410 cm^{-1}, which match signals from the 1,5-DPC spectrum. This is accompanied by the fact that intense signals from the starting 1,5-DPCZ, (e.g. at 688 and 740 cm^{-1}) are not present in the spectrum of the functionalized material. In addition, it can be qualitatively observed that the peak intensity at 1430 and 1583 cm^{-1} for GQDs is reduced after the functionalization (taking the band at 880 cm^{-1} as a reference), which could indicate a decrease in the number of epoxide and carbonyl groups, as a consequence of nucleophilic attacks from 1,5-DPC. Furthermore, the spectrum of the starting 1,5-DPCZ significantly differs from the spectrum obtained for the reaction by-product/s, thus indicating that changes in the structure of the reactant occurred during the process. This chemical modification has been reported for 1,5-DPCZ, and involves its oxidation to 1,5-DPC [33], which is consistent with the change in color observed during the functionalization of GQDs. So far, based on the above observations, the successful functionalization of the GQDs is most likely expected.

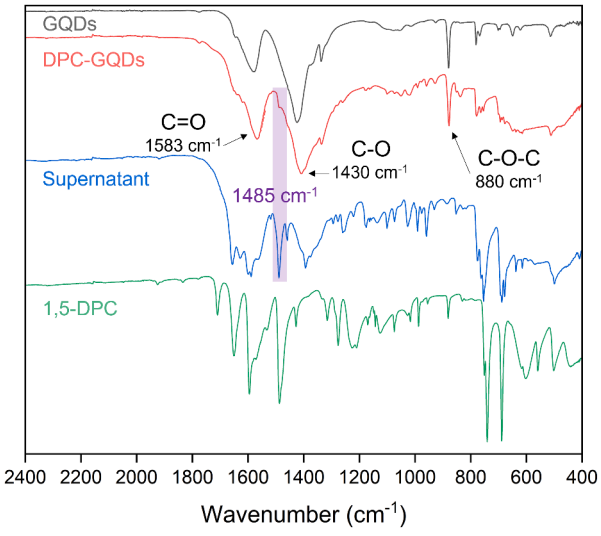

Fig. 2. ATR-FT-IR spectra of graphene quantum dots (GQDs), 1,5-diphenylcarbazone-functionalized GQDs (DPC-GQDs), the dried supernatant obtained from the reaction between GQDs and 1,5-diphenylcarbazide (1,5-DPC). No relevant signals, beside C—H peaks at around 3000 cm^{-1}, were found beyond the shown wavenumbers range.

Excitation-emission matrices (EEMs, also known as 3D fluorescence spectra) were also obtained for the GQDs before and after functionalization with 1,5-DPC, as shown in Fig. 3. In addition, normalized excitation and emission spectra for GQDs and DPC-GQDs can be found in Fig. A1 along with their absorption spectra in Fig. A2, both as part of the Appendix. The spectra show that the as-obtained GQDs present maximum emission intensities at 313 nm with excitation wavelengths around 222 and 260 nm, while DPC-GQDs show a single emission maximum at 418 nm, when excited at 321 nm. This is also consistent with the fact that the maximum absorption of DPC-GQDs occurs at a higher wavelength than in the case of GQDs (Fig. A2). Furthermore, the EEM of the supernatant of the reaction (which is assumed to be 1,5-DPC) shows emission only when excited with wavelengths over 340 nm, while 1,5-DPCZ does not exhibit any fluorescence whatsoever. This confirms that the optical properties of GQDs are significantly altered as a consequence of their functionalization with 1,5-DPC, and that the observed changes do not come from either free 1,5-DPC or 1,5-DPCZ.

Fluorescence response to Fe^{3+}

Fig. 4 shows the emission spectra of DPC-GQDs aqueous solutions before and after the addition of 5.00 mg L^{-1} Fe^{3+}, taken with an excitation wavelength of 321 nm. As can be observed, a significant drop in the emission intensity of the probe occurred upon addition of the analyte, indicating its rapid response. It is important to notice that not only a 61% reduction in the emission intensity was obtained after the addition of Fe^{3+}, but also that the maximum emission wavelength shifted from 421.3 to 428.4 nm. This result confirms that as-synthesized DPC-GQDs act as a fluorescence probe toward Fe^{3+}, due to the ability of the analyte to quench their emission.

On the other hand, the observed red-shift suggests an electron-transfer mechanism as the one responsible for the fluorescence quenching. This occurs due to the proximity of the metal cation, which accelerates the non-radiative recombination of the generated exciton via an electron transfer step. This, in turn, decreases the HOMO-LUMO gap of the probe, thus reducing the probability of radiative relaxation, and leading to a reduction of the emission intensity and a shift in the emission wavelength [37,38]. The proximity of the Fe^{3+} cations to the surface of the GQDs is ascribed to the chelating interaction with 1,5-DPC molecules immobilized along the surface of the carbogenic core. In addition, the possibility of an aggregation-induced mechanism as the one responsible for the fluorescence drop upon Fe^{3+} addition [23] was ruled out, since quenching has been proved to occur without significant

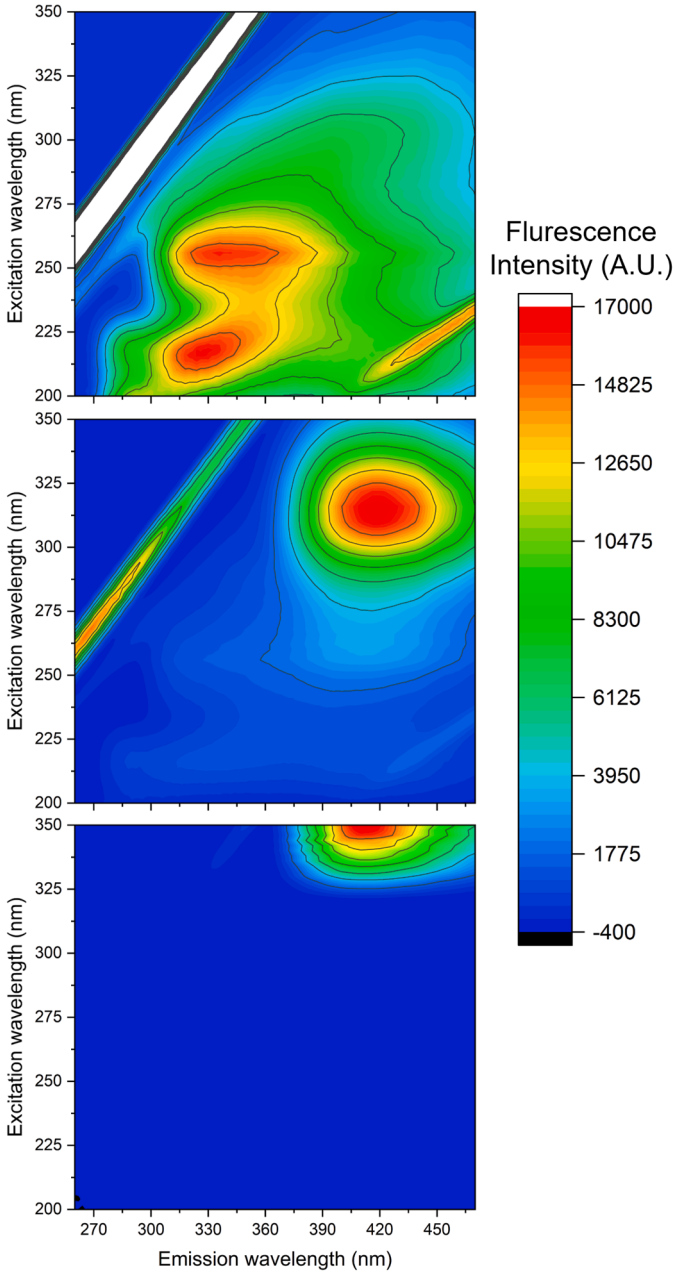

Fig. 3. Excitation-emission matrices for as-synthesized GQDs (top), 1,5-diphenylcarbazone-functionalized GQDs (middle) and 1,5-diphenylcarbazone (bottom). For clarity proposes, the high-intensity emission resulting from scattering (when $\lambda_{em} = \lambda_{exc}$) has been white-colored in the top spectrum.

shifts in the maximum emission wavelength in these cases [39,40].

To quantify the quenching caused by Fe^{3+}, we evaluated the Stern-Volmer model [41], which proposes a mathematical solution of how emission changes as a function of the quencher concentration in the form:

$$\frac{I_0}{I} = 1 + K_{SV}[Q] \quad (1)$$

where; I_0/I represents the ratio between the maximum emission intensity of the probe before and after the addition of the quencher, K_{SV} is the Stern-Volmer constant, which depends on the quenching rate constant and the fluorescence lifetime of the probe in absence of quencher, and *[Q]* is the concentration of quencher. Hence, this model provides a simple and linear relationship between the ratio of intensities and the

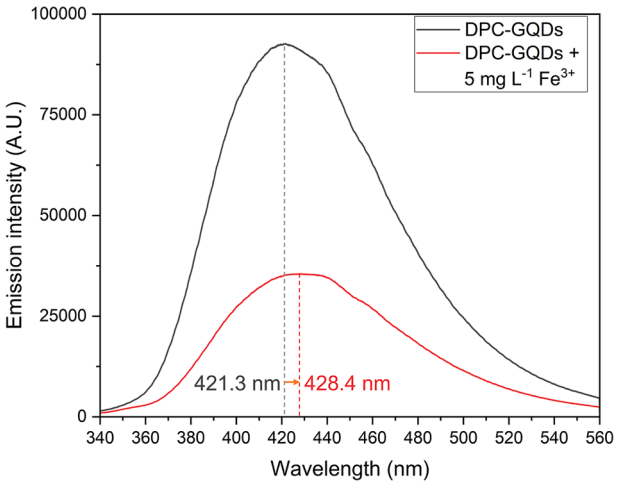

Fig. 4. Emission spectra for a 0.030 mg mL^{-1} solution of 1,5-diphenylcarbazone-functionalized graphene quantum dots (DPC-GQDs) before and after the addition of 5.00 mg L^{-1} of Fe^{3+}.

concentration of Fe^{3+}, ideal for the quantification of the analyte.

With certain understanding of general aspects associated with quenching by Fe^{3+}, we also evaluated and optimized other parameters related to the quantification of this species. Initially, an evaluation of Fe^{3+} calibration curves (from 0.050 to 5.00 mg L^{-1}) obtained using different concentrations of DPC-GQDs was carried out, to assess the effect of the concentration of the probe on the linearity of the detection. Considering the coefficient of determination (R^2) of the linear regressions, we observed that concentrations of DPC-GQDs above 0.030 mg mL^{-1} led to R^2 values higher than 0.989, which is considered adequate for quantification, whereas concentrations below 0.030 mg mL^{-1} resulted in calibration curves with poor linearity. Therefore, concentrations of 0.030 mg mL^{-1} or above of DPC-GQDs were implemented for further experiments.

Other important aspects to consider

To gain insights into the potential degradation and optimal storage conditions, the stability of DPC-GQD solutions was studied. Fig. A3 in the ESI shows the absolute emission intensity of 0.030 mg mL^{-1} solutions obtained from a single stock solution as a function of time, for a period of 40 days. This experiment demonstrates that the stock solution stands for long periods of time with no apparent changes on its emission characteristics.

Additionally, 0.030 mg mL^{-1} solutions of the functionalized probe were subjected to bleaching assays using a commercial UV lamp (15 W, UVC, maximum emission at 253.7 nm), which demonstrated 12 and 25% reductions in their maximum emission intensity after irradiating for 10 and 60 min, respectively. However, this is not considered critical, since the probe was never exposed to prolonged times under UV irradiation other than during the fluorescence sensing.

An additional aspect to consider is the general performance of the DPC-GQDs probe and its emission characteristics in the presence of different salt concentrations. To test this, various concentrations of model saline compound solutions prepared with $NaNO_3$ were mixed with 0.030 mg mL^{-1} DPC-GQDs. Considering ± 5% changes in the original fluorescence as acceptable, Fig. A4 in the Appendix shows that concentrations up to 2.00 g L^{-1} of $NaNO_3$ were suitable for direct application, whereas concentrations above this threshold considerably affected the emission of the probe. This agrees well with the results obtained for real aqueous samples, in which relatively low salinity within waters could be efficiently analyzed by the developed method.

Finally, as part of the optical characterization of the synthesized probe, its response time was also studied. Fig. A5 in the Appendix shows

the emission intensity of DPC-GQDs solutions (0.030 mg mL^{-1}) as a function of the elapsed time upon the addition of 5.00 mg L^{-1} Fe^{3+}. The inset in the figure exhibits a sudden drop in emission intensity of the probe within the first 30 s since the addition of the analyte. This represents an interesting advantage toward applications, since it significantly reduces the time of analysis. Fig. A5 also shows that the quenching remained constant for up to 30 min after the addition of the analyte, while measurements performed 24 h later still showed a similar response.

Improved selectivity of DPC-GQDs

Although the analysis of several factors related to the chemical and optical characteristics of DPC-GQDs was discussed in the previous section, the selectivity of the probe still demanded some improvements. Fig. 5 shows the relative emission intensity of GQDs and DPC-GQDs at pH 9.0 in the presence of selected species, which corresponded to the pH were significant changes for Fe(III) were observed. On the other hand, Fig. A6 (Appendix) shows results obtained for pH 1.0 and 7.0 indicating that as-modified GQDs are sensitive to most of the interference ions present in sample. For the sake of simplicity, it is important to point out that only a small fraction of the interfering species was included in Figs. 5 and A6 (Appendix). Actual experiments were carried out also in the presence of Ag^{+}, Fe^{2+}, Ni^{2+}, Co^{2+}, Cr^{3+}, Cr^{6+}, Ba^{2+}, Mn^{2+}, Zn^{2+}, as well as with the anions SO_4^{2-}, NO_3^{-}, HCO_3^{-} Cl^{-} and Br^{-}. The full range of potentially interfering ions measured at pH 9.0 is shown in Fig. A7 (Appendix).

As can be seen in Fig. 5, GQDs at a pH of 9.0 were quite sensitive toward quenching by different species, such as Al^{3+}, Ca^{2+} and Mg^{2+}, being the last two ions very common species within real samples. This demonstrates that the probe without functionalization lacks selectivity, most probably due to non-specific coordination interactions favored by the presence of oxygenated functional groups on the surface and edges of the material, as shown by the ATR-FT-IR characterization. The functionalized DPC-GQDs, on the other hand, provided an excellent selectivity toward Fe^{3+} under these conditions. Furthermore, as is shown in Fig. A6, the selectivity of both DPC-GQDs and GQDs was significantly lower at pH 7.0, while at pH 1.0 the results were similar to those obtained at pH 9.0. Moreover, it was found that the presence of the potential interfering species did not affect the quenching effect of Fe^{3+}, regardless of the pH.

Taking into consideration the previous results, we considered pH 1.0 and 9.0 adequate, in principle, for a selective determination of Fe^{3+}. However, at acidic pH (~1.0) the emission intensity of the probe was significantly quenched in comparison to pH 9.0, making then the basic pH a better choice in terms of sensitivity. The fact that pH 9.0 was optimal is most likely a consequence of the acid-base characteristics of the carbazone group in the structure of 1,5-DPC, which has a pKa of 8.54 [42], favoring interactions with Fe^{3+} over other species while not suffering from quenching by a high concentration of H^{+}. Furthermore, it should be noticed from the results presented in Figs. 5 and A7, that the quenching effect seems to depend on the charge of the species, being species with $a+3$ charge more efficient quenchers than those with $a+2$ charge, and so forth. It is important to mention that several anions commonly found in samples including SO_4^{-}, Cl^{-} and HCO_3^{-} caused no significant modifications on the response of either GQDs or DPC-GQDs. Furthermore, hydroxyl anions did not significantly quench the emission of the nanomaterial at a pH of 9.0, when compared with measurements performed in ultrapure water. This is consistent with the fact that the probe-analyte interaction is of a coordinating character in both cases, which is expected only for cationic species.

Analytical characteristics

Fig. 6 shows the response curve obtained after the analysis of standard Fe^{3+} samples, with the calibration curve from the linear portion of the plot as an inset, and the actual emission spectra for the linear range in the right panel. As seen in the figure, the relative fluorescence intensities increased linearly with the analyte concentration (as a consequence of the quenching produced by Fe^{3+}), flattening for concentrations above 6.4 mg L^{-1} (115 μmol L^{-1}), which indicates the upper limit of the linear range. The linear relationship between the

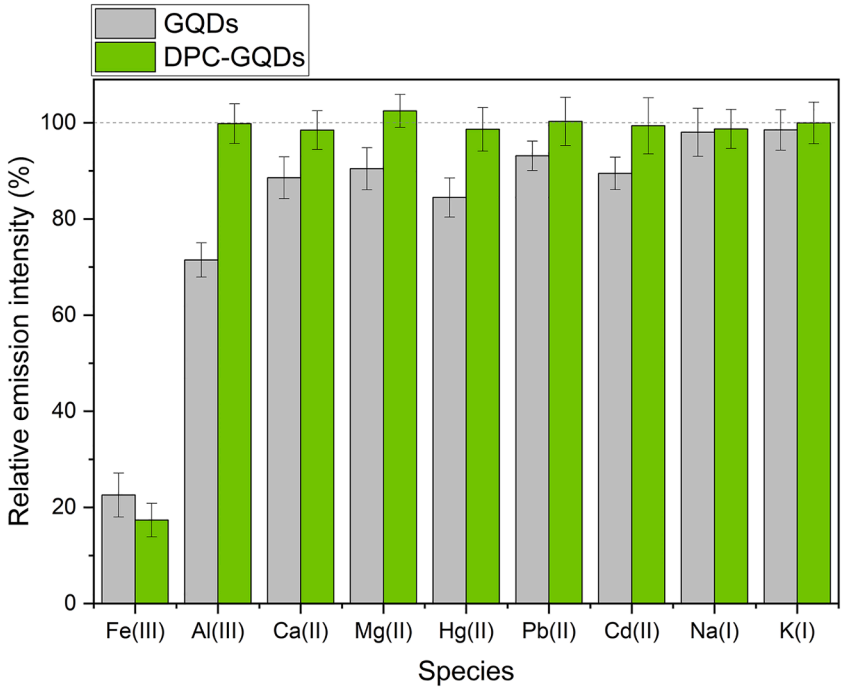

Fig. 5. Relative emission intensity (I/I_0 x 100) for 0.030 mg mL^{-1} for graphene quantum dots (GQDs) and 1,5-diphenylcarbazone-functionalized GQDs (DPC-GQDs) in the presence of 5.00 mg L^{-1} of different ionic species measured at pH 9.0. The maximum emission intensity of pure GQDs and DPC-GQDs were taken as the initial intensity (I_0).

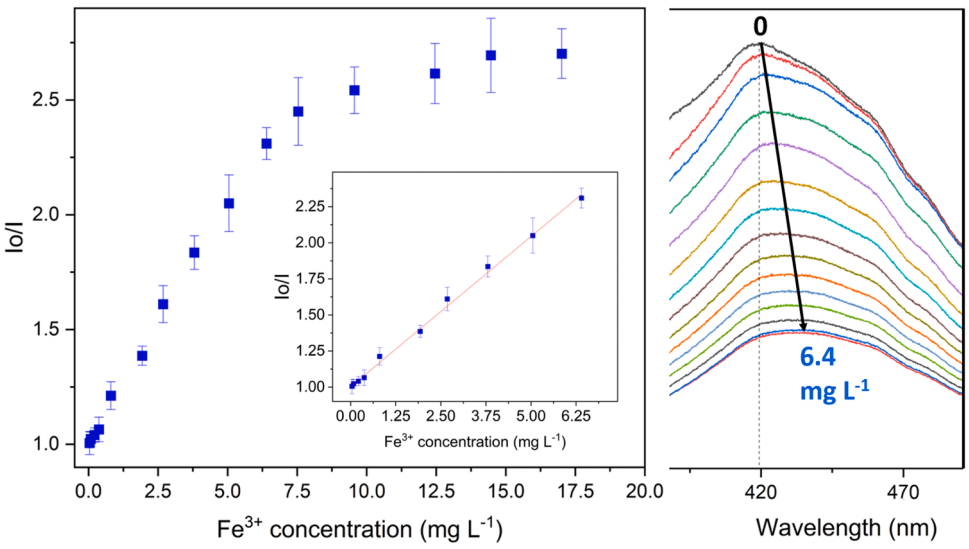

Fig. 6. Relative emission intensity for 0.030 mg mL^{-1} of 1,5-diphenylcarbazide-functionalized graphene quantum dots (DPC-GQDs) as a function of Fe^{3+} concentration, with the linear range shown as an inset ($n = 3$). The panel on the right shows selected emission spectra corresponding to the linear region measured from 0 to 6.4 mg L^{-1}. The vertical dotted line indicates the position of the maximum emission for DPC-GQDs.

relative emission intensity I_0/I and the concentration of $Fe^{3+}$is consistent with the Stern-Volmer model, shown in Eq. (1). From the limit of detection (LOD) to this limit, a linear fit was performed which yielded the equation $Io/I = (1.002 \pm 0.008) + (0.208 \pm 0.004)\ C$, where C is the concentration of Fe^{3+} in mg L^{-1} and Io/I is the relationship between the maximum fluorescence intensity of DPC-GQDs without and with different analyte concentrations. The R^2 correlation coefficient was 0.9962, indicating a fairly acceptable linear fit of the data.

In addition, the linear fit was used to calculate the LOD as 3 times the quotient between the standard deviation of the intercept and the slope as recommended by IUPAC [43]. This resulted in a value of 0.014 mg L^{-1} (0.24 μmol L^{-1}). The limit of quantification was calculated using the same recommendations, as 10 times the aforementioned quotient, yielding a value of 0.047 mg L^{-1} (0.84 μmol L^{-1}). It is important to highlight that the linear range covers most of the expected concentrations of Fe^{3+} in the analyzed samples, and that the LOD is well below the 0.3 mg L^{-1} limit for Fe^{3+} in drinking water, as recommended by the World Health Organization [44]. Moreover, to evaluate the reproducibility of the probe, 6 independent measurements were performed at the optimal conditions with 0.50 mg L^{-1} of Fe^{3+}, resulting in a relative standard deviation of 2.2%, demonstrating an excellent precision. Measurements performed on five different days, on the other hand, yielded a relative standard deviation of 5.7%.

Table 1 summarizes and compares the most recently reported fluorescence GQD-based sensors for Fe species, including ours. The table shows type of fluorescence sensor, synthesis method, linear range, LOD, and the sample source. The LOD achieved with our developed probe is in line with the values obtained in most of the cited works, as well as the linear range. However, for a fair comparison, the sample source should be taken into account in this analysis, since more than half of these recent reports do not include the analysis of real or more complex samples other than drinking water. This is a clear demonstration of the difficulties encountered when applying this type of probes in the context of real-life matrices. Interestingly, there are two recent reports that addressed the application of probes in more complex samples, namely human serum [45] and human urine [46], albeit with significant interferences from several species in both reported probes. Our work, on the other hand, allowed for a highly selective determination of Fe^{3+} in waters and white wines, without major interferences. Furthermore, all of the methods included in the comparison involve bottom-up wet chemistry syntheses of GQDs, which usually require harsh chemical conditions [47] and extensive purification steps (e.g. prolonged dialysis [24,46]). These issues were prevented by our method, which consisted in a simple electrochemical exfoliation from graphene followed by a

Table 1
Comparison of the hereby presented results with other recently published GQD-based fluorescence sensors for Fe^{3+} determination.

Fluorescence Sensor	Synthesis Method	Linear Range	LOD	Real Samples	Refs.
Single-layer GQDs	Hydrothermal	0 – 85 μM	0.26 μM	Tap water	[5]
Er^{3+}-doped GQDs	Hydrothermal	0.04 – 140 μM	11.2 nM	Human serum	[45]
N,Fe-co-doped GQDs	Hydrothermal	10 – 110 μM	3.21 μM	Human serum and urine	[46]
S and N co-doped GQDs	High-temperature pyrolysis	0 – 20 and 200 – 667 μM	41.1 and 500 nM	River water	[47]
N-doped GQDs	Acid vapor cutting	0.50 – 50 μM	Not reported	Tap water	[48]
GQD-embedded hydrogel	Pyrolysis (GQDs)	10 – 200 μM	Not reported	None	[27]
GQDs	Pyrolysis	3.5 – 670 μM	1.6 μM	Tap water	[30]
N-doped GQDs	Hydrothermal	1.6 – 6.0 mM	2.37 μM	None	[26]
N-GQDs-based test paper	Hydrothermal (N-GQDs)	Not reported	0.1 μM	Drinking water	[29]
Glutathione-doped GQDs	Pyrolysis	1 – 150 μM	0.10 μM	Drinking water	[28]
DPC-GQDs	Electrochemical exfoliation from 3D graphene	0.24 – 115 μM (water) 2.0 – 120 μM (wine)	0.24 μM (water) 2.0 μM (wine)	Tap, dam, river and underground waters, white wines	This work

straightforward wet chemistry approach for their functionalization, requiring no further steps than mixing and centrifugation for their purification.

Front-face fluorescence measurements with real samples

Finally, the quantification of Fe^{3+} in different real water samples; namely tap, river, and dam waters, was carried out. Significant drawbacks during the measurements were experienced due to radiation shielding effects caused by the presence of species within the sample matrix, which absorb radiation and affect the excitation-emission process. This resulted especially inconvenient taking into account the fact that the Stern-Volmer expression (Eq. (1)) can only be applied as an external calibration curve, since an analyte-free measurement is required to calculate the relative emission intensity I_0/I, thus ruling out the application of a standard addition calibration. In this context, front-face fluorescence measurements represented a fundamental tool to minimize shielding effects and to obtain spectra from real samples that could be effectively analyzed, thanks to the reduction in the optical path length resulting from this configuration [49].

Consequently, using the front-face fluorescence approach along with optimal chemical conditions, we were able to construct an external calibration curve obtained from synthetic standards (Fig. 6) which was later used for the determination of Fe^{3+} in all of the water samples tested in this work. In addition, to further evaluate the accuracy of the method, standard recovery assays were carried out with all the aqueous samples at two levels: 0.10 and 1.00 mg L^{-1}, as shown in Table 2. The table also shows the results obtained from a standard spectrophotometric method for the determination of Fe^{3+}, based on a liquid-liquid extraction using ethyl acetate, after the addition of KSCN as complexing and chromogenic reagent [50]. The table shows that the developed fluorescence probe yielded results which were in excellent agreement with the highly established colorimetric method used as reference. Furthermore, the results of the recovery assays were satisfactory, with recoveries ranging from 100 to 120% at the 0.10 mg L^{-1} level, and from 97 to 103% at the 1.00 mg L^{-1} level.

Table 2
Determination of Fe^{3+} in waters from various sources and of total Fe in white wines, along with recovery studies (95% confidence interval, $n = 3$). All concentrations are mg L^{-1}.

Water Sample	Fe^{3+} added	Fe^{3+} found DPC-GQDs	Recovery (%)[a]	Fe^{3+} found Spectrophotometric	Recovery (%)[a]
Tap	0	0.44 ± 0.03	–	0.41 ± 0.02	–
	0.10	0.55 ± 0.04	110	0.50 ± 0.03	90
	1.00	1.47 ± 0.06	103	1.42 ± 0.04	101
River	0	0.98 ± 0.04	–	1.01 ± 0.05	–
	0.10	1.08 ± 0.07	100	1.10 ± 0.05	90
	1.00	1.95 ± 0.0	97	2.00 ± 0.07	99
Dam	0	0.77 ± 0.05	–	0.80 ± 0.04	–
	0.10	0.89 ± 0.08	120	0.89 ± 0.03	90
	1.00	1.74 ± 0.05	97	1.75 ± 0.05	95
White wine	Fe^{3+} added	Fe found DPC-GQDs	Recovery (%)[a]	Fe found Spectrophotometric	Recovery (%)[a]
Sample 1	0	1.65 ± 0.11	–	1.71 ± 0.05	–
	1.00	2.56 ± 0.09	91	2.77 ± 0.04	106
Sample 2	0	1.11 ± 0.09	–	1.13 ± 0.05	–
	1.00	2.20 ± 0.12	109	2.15 ± 0.07	102
Sample 3	0	2.03 ± 0.16	–	2.18 ± 0.10	–
	1.00	3.00 ± 0.15	97	2.08 ± 0.15	90

[a] Recovery = 100 x (Found – Initial) / Added.

Moreover, to demonstrate the sensing capabilities of the developed DPC-GQDs in more complex samples than water, the analysis of white wines was carried out. Since direct measurements were not possible in this case due to the high organic content within the matrix sample, we added a digestion step to the overall protocol. Typical digestion procedures for elemental analysis involve high concentrations of acids (i.e.; HNO_3) and/or oxidants [51–53], which resulted impractical for fluorescence measurements using GQDs, since the probe readily oxidizes under these conditions. The *Collection of Real Samples and Treatment* section describes the soft digestion protocol performed in this work. This finally led to solutions easily buffered to pH 9.0. In this case, the oxidizing medium (needed for the soft digestion) resulted in the oxidation of Fe^{2+} to Fe^{3+}, leading to the quantification of total Fe in wine samples. This was ultimately achieved using matrix-matched standard solutions obtained by treating aqueous standards with the described digestion protocol. Considering this, the analytical figures of merit for the determination of Fe in these samples were different from those obtained for the analysis of waters. Based on the calibration curve, a LOD of 0.11 mg L^{-1} (2.0 μmol L^{-1}) and a linear range up to 6.7 mg L^{-1} (120 μmol L^{-1}) were obtained. These are useful values considering the usual concentrations of Fe in white wines [54], and were corroborated by the application of the probe on these samples, as shown in Table 2. The table also shows the concentrations of Fe in the same samples, determined by the application of a spectrophotometric method developed by Riganakos et al. [55]. As can be seen, these do not significantly differ from those obtained using the fluorescence probe. Furthermore, recovery studies were carried out using 1.00 mg L^{-1} Fe^{3+} standard additions, with adequate results ranging between 91 and 109%.

Conclusions

A sensitive, selective, and fast fluorescence probe has been developed on the basis of electrochemically-obtained GQDs further functionalized with 1,5-DPC, for the determination of Fe species in standard and real samples. The clean and straightforward electrochemical approach led to small and highly crystalline carbon nanostructures without the need of using harsh chemicals and performing tedious purification steps such as cleaning and dialysis protocols. Although as-synthesized GQDs presented very good sensitivity, they lacked of selectivity toward the analyte of interest. Consequently, 1,5-DPC-functionalized GQDs significantly improved the selectivity of the probe toward Fe^{3+} and allowed for its specific determination after carefully optimizing both chemical and instrumental parameters. We also incorporated the use of front-face fluorescence to eliminate shielding effects caused by radiation. The developed probe gave a full response toward the analyte in less than 30 s and the aqueous solutions were stable for over 40 days under regular storage conditions. Importantly, the probe was successfully applied for the determination of Fe within wine beverages with an LOD of 2.0 μmol L^{-1} and a linear range up to 120 μmol L^{-1}. White wines represented a specially challenging sample, since matrix effects usually hinder the application of GQD-based probes for the analysis of samples other than waters. To overcome this issue, a soft UV light-based digestion was optimized which, along with the development of a matrix-matched calibration curve, allowed for the desired analysis. Finally, one of the main highlights of this work relays on the fluorescence detection of Fe in real samples employing a simple and reliable method. In summary, the developed functional nanomaterial

permitted the determination of Fe in complex samples which are usually beyond reach for GQD-based fluorescence probes.

Funding

This research was funded by Consejo Nacional de Investigaciones Científicas y Técnicas (CONICET), Agencia Nacional de Promoción Científica y Tecnológica (FONCYT) (Projects PICT-2016-2506-BID, PICT-2019-03859-BID, PICT-2019-2188) and Universidad Nacional de Cuyo (Project 06/M129) (Argentina).

CRediT authorship contribution statement

Mauricio Llaver: Conceptualization, Data curation, Formal analysis, Investigation, Validation, Visualization, Writing – original draft. **Santiago D. Barrionuevo:** Data curation, Formal analysis, Investigation. **Horacio Troiani:** Investigation. **Rodolfo G. Wuilloud:** Resources, Project administration, Funding acquisition. **Francisco J. Ibañez:** Conceptualization, Resources, Writing – review & editing, Supervision, Project administration, Funding acquisition.

Declaration of Competing Interest

The authors declare that they have no known competing financial interests or personal relationships that could have appeared to influence the work reported in this paper.

Data availability

Data will be made available on request.

Supplementary materials

Supplementary material associated with this article can be found, in the online version, at doi:10.1016/j.talo.2023.100202.

References

[1] S.-.Y. Li, L. He, Recent progresses of quantum confinement in graphene quantum dots, Front. Phys. 17 (2022) 33201, https://doi.org/10.1007/s11467-021-1125-2.
[2] V. Kansara, R. Shukla, S.J.S. Flora, P. Bahadur, S. Tiwari, Graphene quantum dots: synthesis, optical properties and navigational applications against cancer, Mater. Today Commun. 31 (2022), 103359, https://doi.org/10.1016/j.mtcomm.2022.103359.
[3] N. Zahir, P. Magri, W. Luo, J.J. Gaumet, P. Pierrat, Recent advances on graphene quantum dots for electrochemical energy storage devices, Energy Environ. Mater. 5 (2022) 201–214, https://doi.org/10.1002/eem2.12167.
[4] S. Zhou, H. Xu, W. Gan, Q. Yuan, Graphene quantum dots: recent progress in preparation and fluorescence sensing applications, RSC Adv. 6 (2016) 110775–110788, https://doi.org/10.1039/C6RA24349E.
[5] H. Wang, X. Wu, W. Dong, S.-.L. Lee, Q. Yuan, W. Gan, One-step preparation of single-layered graphene quantum dots for the detection of Fe3+, Spectrochim. Acta. A. Mol. Biomol. Spectrosc. 226 (2020), 117626 https://doi.org/10.1016/j.saa.2019.117626.
[6] M.K. Chini, V. Kumar, A. Javed, S. Satapathi, Graphene quantum dots and carbon nano dots for the FRET based detection of heavy metal ions, Nano-Struct. Nano-Obj. 19 (2019), 100347, https://doi.org/10.1016/j.nanoso.2019.100347.
[7] P. Naksen, S. Boonruang, N. Yuenyong, H.L. Lee, P. Ramachandran, W. Anutrasakda, M. Amatatongchai, S. Pencharee, P. Jarujamrus, Sensitive detection of trace level Cd (II) triggered by chelation enhanced fluorescence (CHEF) "turn on": nitrogen-doped graphene quantum dots (N-GQDs) as fluorometric paper-based sensor, Talanta 242 (2022), 123305, https://doi.org/10.1016/j.talanta.2022.123305.
[8] S. Zhu, X. Bai, T. Wang, Q. Shi, J. Zhu, B. Wang, One-step synthesis of fluorescent graphene quantum dots as an effective fluorescence probe for vanillin detection, RSC Adv. 11 (2021) 9121–9129, https://doi.org/10.1039/d0ra10825a.
[9] S.A. Prabhu, V. Kavithayeni, R. Suganthy, K. Geetha, Graphene quantum dots synthesis and energy application: a review, Carbon Lett. 31 (2021) 1–12, https://doi.org/10.1007/s42823-020-00154-w.
[10] W.H. Danial, N.A. Norhisham, A.F. Ahmad Noorden, Z. Abdul Majid, K. Matsumura, A. Iqbal, A short review on electrochemical exfoliation of graphene and graphene quantum dots, Carbon Lett. 31 (2021) 371–388, https://doi.org/10.1007/s42823-020-00212-3.
[11] M.M. Messina, S.D. Barrionuevo, M.E. Coustet, M.P. Kreuzer, F.D. Saccone, P.C. dos Santos Claro, F.J. Ibañez, Graphene and carbon dots for photoanodes with enhanced performance, ACS Appl. Nano Mater. 4 (2021) 7309–7318, https://doi.org/10.1021/acsanm.1c01295.
[12] I. Matsumoto, R. Sekiya, T. Haino, A protocol for size separation of nanographenes, RSC Adv. 9 (2019) 33843–33846, https://doi.org/10.1039/C9RA07528C.
[13] M.A. Sk, A. Ananthanarayanan, L. Huang, K.H. Lim, P. Chen, Revealing the tunable photoluminescence properties of graphene quantum dots, J. Mater. Chem. C 2 (2014) 6954–6960, https://doi.org/10.1039/C4TC01191K.
[14] I.A. Revesz, S.M. Hickey, M.J. Sweetman, Metal ion sensing with graphene quantum dots: detection of harmful contaminants and biorelevant species, J. Mater. Chem. B 10 (2022) 4346–4362, https://doi.org/10.1039/D2TB00408A.
[15] S. Tachi, H. Morita, M. Takahashi, Y. Okabayashi, T. Hosokai, T. Sugai, S. Kuwahara, Quantum yield enhancement in graphene quantum dots via esterification with benzyl alcohol, Sci. Rep. 9 (2019) 14115, https://doi.org/10.1038/s41598-019-50666-3.
[16] B. Zhang, Y. He, Z. Fan, Nitrogen-doped graphene quantum dots as highly sensitive and selective fluorescence sensor detection of iodide ions in milk powder, J. Photochem. Photobiol. Chem. 367 (2018) 452–457, https://doi.org/10.1016/j.jphotochem.2018.09.014.
[17] Z. Yu, W. Ma, T. Wu, J. Wen, Y. Zhang, L. Wang, Y. He, H. Chu, M. Hu, Coumarin-modified graphene quantum dots as a sensing platform for multicomponent detection and its applications in fruits and living cells, ACS Omega 5 (2020) 7369–7378, https://doi.org/10.1021/acsomega.9b04387.
[18] L. Li, G. Wu, T. Hong, Z. Yin, D. Sun, E.S. Abdel-Halim, J.-.J. Zhu, Graphene quantum dots as fluorescence probes for turn-off sensing of melamine in the presence of Hg2+, ACS Appl. Mater. Interfaces. 6 (2014) 2858–2864, https://doi.org/10.1021/am405305r.
[19] W. Wang, S. Xu, N. Li, Z. Huang, B. Su, X. Chen, Sulfur and phosphorus co-doped graphene quantum dots for fluorescent monitoring of nitrite in pickles, Spectrochim. Acta. A. Mol. Biomol. Spectrosc. 221 (2019), 117211, https://doi.org/10.1016/j.saa.2019.117211.
[20] G. Drava, V. Minganti, Mineral composition of organic and conventional white wines from Italy, Heliyon 5 (2019) e02464, https://doi.org/10.1016/j.heliyon.2019.e02464.
[21] P. Pohl, What do metals tell us about wine? TrAC Trends Anal. Chem. 26 (2007) 941–949, https://doi.org/10.1016/j.trac.2007.07.005.
[22] W.N.L. dos Santos, G.C. Brandão, L.A. Portugal, J.M. David, S.L.C. Ferreira, A photo-oxidation procedure using UV radiation/H2O2 for decomposition of wine samples — Determination of iron and manganese content by flame atomic absorption spectrometry, Spectrochim. Acta Part B At. Spectrosc. 64 (2009) 601–604, https://doi.org/10.1016/j.sab.2009.04.012.
[23] A. Ananthanarayanan, X. Wang, P. Routh, B. Sana, S. Lim, D.-.H. Kim, K.-.H. Lim, J. Li, P. Chen, Facile synthesis of graphene quantum dots from 3D graphene and their application for Fe3+ sensing, Adv. Funct. Mater. 24 (2014) 3021–3026, https://doi.org/10.1002/adfm.201303441.
[24] S.K. Raj, A. Rajput, H. Gupta, R. Patidar, V. Kulshrestha, Selective recognition of Fe3+ and Cr3+ in aqueous medium via fluorescence quenching of graphene quantum dots, J. Dispers. Sci. Technol. 40 (2019) 250–255, https://doi.org/10.1080/01932691.2018.1467775.
[25] C. Zhang, Y. Cui, L. Song, X. Liu, Z. Hu, Microwave assisted one-pot synthesis of graphene quantum dots as highly sensitive fluorescent probes for detection of iron ions and pH value, Talanta 150 (2016) 54–60, https://doi.org/10.1016/j.talanta.2015.12.015.
[26] F. Lu, Y.-.H. Zhou, L.-.H. Wu, J. Qian, S. Cao, Y.-.F. Deng, Y. Chen, Highly fluorescent nitrogen-doped graphene quantum dots' synthesis and their applications as Fe(III) ions sensor, Int. J. Opt. 2019 (2019), 8724320, https://doi.org/10.1155/2019/8724320.
[27] D.W.M. Pincher, C.A. Bader, J.D. Hayball, S.E. Plush, M.J. Sweetman, Graphene quantum dot embedded hydrogel for dissolved iron sensing, ChemistrySelect 4 (2019) 9640–9646, https://doi.org/10.1002/slct.201901779.
[28] K. Saenwong, P. Nuengmatcha, P. Sricharoen, N. Limchoowong, S. Chanthai, GSH-doped GQDs using citric acid rich-lime oil extract for highly selective and sensitive determination and discrimination of Fe3+ and Fe2+ in the presence of H2O2 by a fluorescence "turn-off" sensor, RSC Adv 8 (2018) 10148–10157, https://doi.org/10.1039/c7ra13432k.
[29] C. Wang, Y. Sun, J. Jin, Z. Xiong, D. Li, J. Yao, Y. Liu, Highly selective, rapid-functioning and sensitive fluorescent test paper based on graphene quantum dots for on-line detection of metal ions, Anal. Methods 10 (2018) 1163–1171, https://doi.org/10.1039/c7ay02995k.
[30] Y. Zhang, X. Yang, Y. Pu, W. Cheng, S. Lin, Z. Shao, X. Liao, Selective, sensitive and label-free detection of Fe3+ ion in tap water using highly fluorescent graphene quantum dots, J. Fluoresc. 29 (2019) 541–548, https://doi.org/10.1007/s10895-019-02365-5.
[31] X. Li, W. Cai, J. An, S. Kim, J. Nah, D. Yang, R. Piner, A. Velamakanni, I. Jung, E. Tutuc, S.K. Banerjee, L. Colombo, R.S. Ruoff, Large-area synthesis of high-quality and uniform graphene films on copper foils, Science 324 (2009) 1312–1314, https://doi.org/10.1126/science.1171245.
[32] M. Llaver, S.D. Barrionuevo, E. Prieto, R.G. Wuilloud, F.J. Ibañez, Functionalized graphene quantum dots obtained from graphene foams used for highly selective detection of Hg2+ in real samples, Anal. Chim. Acta 1232 (2022), 340422, https://doi.org/10.1016/j.aca.2022.340422.
[33] A. Shishov, P. Terno, L. Moskvin, A. Bulatov, In-syringe dispersive liquid-liquid microextraction using deep eutectic solvent as disperser: determination of chromium (VI) in beverages, Talanta 206 (2020), 120209, https://doi.org/10.1016/j.talanta.2019.120209.

[34] M. Ahmad, B. Zhang, J. Wang, J. Xu, K. Manzoor, S. Ahmad, S. Ikram, New method for hydrogel synthesis from diphenylcarbazide chitosan for selective copper removal, Int. J. Biol. Macromol. 136 (2019) 189–198, https://doi.org/10.1016/j.ijbiomac.2019.06.084.
[35] J.C. Meyer, A.K. Geim, M.I. Katsnelson, K.S. Novoselov, D. Obergfell, S. Roth, C. Girit, A. Zettl, On the roughness of single- and bi-layer graphene membranes, Solid State Commun. 143 (2007) 101–109, https://doi.org/10.1016/j.ssc.2007.02.047.
[36] L. Centeno, J. Romero-García, C. Alvarado-Canché, C. Gallardo-Vega, G. Télles-Padilla, E. Díaz Barriga-Castro, E.N. Cabrera-Álvarez, A. Ledezma-Pérez, A. de León, Green synthesis of graphene quantum dots from Opuntia sp. extract and their application in phytic acid detection, Sens. Bio-Sens. Res. 32 (2021), 100412, https://doi.org/10.1016/j.sbsr.2021.100412.
[37] T. Anusuya, V. Kumar, V. Kumar, Hydrophilic graphene quantum dots as turn-off fluorescent nanoprobes for toxic heavy metal ions detection in aqueous media, Chemosphere 282 (2021), 131019, https://doi.org/10.1016/j.chemosphere.2021.131019.
[38] Z. Xiaoyan, L. Zhangyi, L. Zaijun, Fabrication of valine-functionalized graphene quantum dots and its use as a novel optical probe for sensitive and selective detection of Hg2+, Spectrochim. Acta. A. Mol. Biomol. Spectrosc. 171 (2017) 415–424, https://doi.org/10.1016/j.saa.2016.08.037.
[39] N. Wang, Z.X. Liu, R.S. Li, H.Z. Zhang, C.Z. Huang, J. Wang, The aggregation induced emission quenching of graphene quantum dots for visualizing the dynamic invasions of cobalt(II) into living cells, J. Mater. Chem. B 5 (2017) 6394–6399, https://doi.org/10.1039/C7TB01316G.
[40] X. Zhu, J. Liu, H. Peng, J. Jiang, R. Yu, A novel fluorescence assay for inorganic pyrophosphatase based on modulated aggregation of graphene quantum dots, Analyst 141 (2015) 251–255, https://doi.org/10.1039/C5AN01937K.
[41] M.H. Gehlen, The centenary of the Stern-Volmer equation of fluorescence quenching: from the single line plot to the SV quenching map, J. Photochem. Photobiol. C Photochem. Rev. 42 (2020), 100338, https://doi.org/10.1016/j.jphotochemrev.2019.100338.
[42] K.L. Cheng, K. Ueno, T. Imamura, CRC Handbook of Organic Analytical Reagents, Routledge, 2017.
[43] V. Gold, The IUPAC compendium of chemical terminology. The Gold Book, 4th ed., International Union of Pure and Applied Chemistry (IUPAC), Research Triangle Park, NC, 2019 https://doi.org/10.1351/goldbook.
[44] G.C. Ghosh, Md.J.H. Khan, T.K. Chakraborty, S. Zaman, A.H.M.E. Kabir, H. Tanaka, Human health risk assessment of elevated and variable iron and manganese intake with arsenic-safe groundwater in Jashore, Bangladesh, Sci. Rep. 10 (2020) 5206, https://doi.org/10.1038/s41598-020-62187-5.
[45] T.V. Huynh, N.T.N. Anh, W. Darmanto, R.-.A. Doong, Erbium-doped graphene quantum dots with up- and down-conversion luminescence for effective detection of ferric ions in water and human serum, Sens. Actuators B Chem. (2021) 328, https://doi.org/10.1016/j.snb.2020.129056.
[46] X.X. Gao, X. Zhou, Y.F. Ma, C.P. Wang, F.X. Chu, A fluorometric and colorimetric dual-mode sensor based on nitrogen and iron co-doped graphene quantum dots for detection of ferric ions in biological fluids and cellular imaging, New J. Chem. 42 (2018) 14751–14756, https://doi.org/10.1039/c8nj01805g.
[47] Y.-.P. Zhang, J.-.M. Ma, Y.-.S. Yang, J.-.X. Ru, X.-.Y. Liu, Y. Ma, H.-.C. Guo, Synthesis of nitrogen-doped graphene quantum dots (N-GQDs) from marigold for detection of Fe 3+ ion and bioimaging, Spectrochim. Acta Part Mol. Biomol. Spectrosc. 217 (2019) 60–67, https://doi.org/10.1016/j.saa.2019.03.044.
[48] H. Xu, S. Zhou, W. Fang, Y. Fan, Synthesis of N-doped graphene quantum dots from bulk N-doped carbon nanofiber film for fluorescence detection of Fe3+ and ascorbic acid, Fuller. Nanotub. Carbon Nanostruct. 29 (2020) 218–226, https://doi.org/10.1080/1536383X.2020.1831474.
[49] D. Airado-Rodríguez, I. Durán-Merás, T. Galeano-Díaz, J.P. Wold, Front-face fluorescence spectroscopy: a new tool for control in the wine industry, J. Food Compos. Anal. 24 (2011) 257–264, https://doi.org/10.1016/j.jfca.2010.10.005.
[50] Z. Marczenko, M. Balcerzak, Chapter 26 - iron, in: Z. Marczenko, M. Balcerzak (Eds.), Chapter 26 - iron, Anal. Spectrosc. Libr. (2000) 226–237, https://doi.org/10.1016/S0926-4345(00)80090-5.
[51] K. Greda, P. Pohl, Direct analysis of wines from the province of Lower Silesia (Poland) by microplasma source optical emission spectrometry, Food Chem. 371 (2022), 131178, https://doi.org/10.1016/j.foodchem.2021.131178.
[52] R.A. Cruz Junior, A.V.B. Chagas, C.S.A. Felix, R.C. Souza, L.A. Silva, V.A. Lemos, S. L.C. Ferreira, A closed inline system for sample digestion using 70% hydrogen peroxide and UV radiation. Determination of lead in wine employing ETAAS, Talanta 191 (2019) 479–484, https://doi.org/10.1016/j.talanta.2018.08.085.
[53] R. Cellier, S. Berail, J. Barre, E. Epova, F. Claverie, A.-.L. Ronzani, S. Milcent, P. Ors, O.F.X. Donard, Analytical strategies for Sr and Pb isotopic signatures by MC-ICP-MS applied to the authentication of Champagne and other sparkling wines, Talanta 234 (2021), 122433, https://doi.org/10.1016/j.talanta.2021.122433.
[54] M. Olalla, M.C. González, C. Cabrera, M.C. López, Optimized determination of iron in grape juice, wines, and other alcoholic beverages by atomic absorption spectrometry, J. AOAC Int. 83 (2000) 189–195, https://doi.org/10.1093/jaoac/83.1.189.
[55] K.A. Riganakos, P.G. Veltsistas, Comparative spectrophotometric determination of the total iron content in various white and red Greek wines, Food Chem. 82 (2003) 637–643, https://doi.org/10.1016/S0308-8146(03)00120-1.